JOURNAL OF MOLECULAR SPECTROSCOPY **143**, 61–80 (1990)

Calculated Rotational and Rovibrational Spectra of D_2S and HDS

STEVEN MILLER AND JONATHAN TENNYSON

Department of Physics and Astronomy, University College London, Gower St., London WC1E 6BT, United Kingdom

PAVEL ROSMUS AND JORG SENEKOWITSCH

Fachbereich Chemie, Universitat Frankfurt, D-6000 Frankfurt, Federal Republic of Germany

AND

IAN M. MILLS

Department of Chemistry, University of Reading, Whiteknights, Reading RG6 2AD, United Kingdom

Rovibrational energy levels, transition frequencies, and linestrengths are computed variationally for the sulfur hydrides D_2S and HDS, using ab initio potential energy and dipole surfaces. Wavenumbers for the pure rotational transitions agree to within 0.2 cm^{-1} of the experimental lines. For the fundamental vibrational transitions, the band origins for D_2S are 860.4, 1900.6, and 1912.0 cm^{-1} for ν_2, ν_1, and ν_3, respectively, compared with the corresponding experimental values of 855.4, 1896.4, and 1910.2 cm^{-1}. For HDS, we compute ν_2 to be 1039.4 cm^{-1}, compared with the experimental value of 1032.7 cm^{-1}. The relative merits of local and normal mode descriptions for the overtone stretching band origins are discussed. Our results confirm the local mode nature of the H_2S, D_2S, and HDS system.

1. INTRODUCTION

In recent ab initio studies we have generated potential energy and dipole surfaces for H_2S (*1*) which yielded fundamental vibrational band origins within 8 cm^{-1} of those measured experimentally (*2*). The 20 overtone and combination bands measured up to 10 000 cm^{-1} all agreed with the calculated values to within 20 cm^{-1}. The calculated equilibrium bond length and angle differed from the experimental values (*3*) by less than 0.2% resulting in the leading rotational constants, A, B, and C, being reproduced to within 2%.

The dipole surface, however, did not give quite such satisfactory results. A comparison of the experimental ν_2 bending fundamental spectrum measured by Mills (*4*) and that computed by Senekowitsch *et al.* (*1*) showed good agreement, after correction for the difference in band origins was made. But the dipole surface is extremely flat with respect to the stretching coordinates (ν_1, symmetric stretch, and ν_3, asymmetric stretch) and the intensities of these modes could not be so well reproduced.

In the last 4 years, there have been a number (*5, 6*) of experimental studies of the pure rotational and rovibrational spectra of the deuterated isotopomer D_2S. The pure

0022-2852/90 $3.00

rotational spectrum of the mixed species HDS has also been measured (*5*). Accurate intensity measurements accompanied the pure rotational spectra. Recently a limited study of the ν_2 band of HDS has been reported (*7*). There is, however, far less experimental data on the deuterated species than for H_2S itself. A theoretical study of the deuterated isotopomers is useful, therefore, not only to see how well the theoretical surfaces reproduce the experimental data but also to make predictions for those bands not already investigated in the laboratory.

2. COMPUTATIONAL DETAILS

2.1. Rovibrational Energy Levels and Wavefunctions

The potential energy and dipole surfaces are fits to 50 values calculated for near-equilibrium geometries using 156 Gaussian-type orbitals using the coupled electron pair approximation (CEPA). Further details of the surfaces may be found in Ref. (*1*). Perturbation theory was used in the analysis of the potential energy surface (*1*) to derive spectroscopic constants.

Fully coupled, variational rovibrational energy levels, transition wavenumbers, and linestrengths were computed using the TRIATOM program suite. These programs have recently been upgraded (*8*) for any general combination of two radial coordinates and the included angle, independent of the coordinate system in which the potential energy surface may be expressed.

For these calculations, Radau coordinates (q_1, q_2, θ) (*9*) were used to represent the molecular structure even though the potential is written in bond-length, bond-angle coordinates. Radau coordinates are shown in Fig. 1. q_1 is the distance between atom $\mathbf{A}_2$ and the point **R**; q_2 is the distance between atom $\mathbf{A}_1$ and the point **P**. Then g_1 and g_2 are the ratios of distances defined by

$$g_1 = \frac{\mathbf{P} - \mathbf{A}_3}{\mathbf{A}_2 - \mathbf{A}_3}, \tag{1}$$

and

$$g_2 = \frac{\mathbf{R} - \mathbf{A}_3}{\mathbf{A}_1 - \mathbf{A}_3}.$$

In the case that the molecule has C_{2v} symmetry, $g_1 = g_2$.

For Radau coordinates,

$$g_1 = \frac{\alpha}{\alpha + \beta - \alpha\beta}, \tag{2}$$

and

$$g_2 = \frac{\alpha}{1 - \beta + \alpha\beta},$$

where

$$\alpha = \left(\frac{m_3}{m_1 + m_2 + m_3}\right)^{1/2}, \tag{3}$$

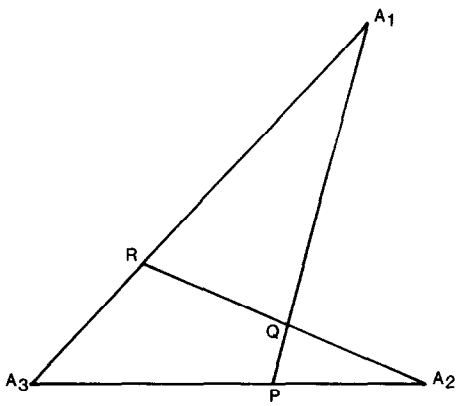

FIG. 1. Coordinate system used in the TRIATOM program suite.

and

$$\beta = \frac{m_2}{m_1 + m_2},$$

and m_1, etc., are the masses of the respective atoms.

For D_2S and HDS, m_3 is much larger than the other two atomic masses. For D_2S, $g_1 = g_2 = 0.0297$, and for HDS, with H at atom A_1, $g_1 = 0.0299$ and $g_2 = 0.0152$. Thus Radau coordinates differ very little from the bond-length, bond-angle coordinates in which the potential is written and the two sets of coordinates are related by a simple transformation. However, the Radau coordinates are orthogonal (*10*), a fact which leads to considerable computational efficiency when computing rotationally excited states.

Basis functions for the calculations consisted of products of Morse oscillator-type functions in q_1 and q_2 and Legendre polynomials in $\cos(\theta)$. For the $J = 0$ band origins, a basis set composed of 1600 functions chosen on energy ordering (*8*) was used. For H_2S and D_2S, we also used the option to symmetrize the q_1, q_1 basis functions. This splits the calculation into two sets of basis functions, one with a *symmetric* combination, the other with an *antisymmetric* combination; thus

$$\Phi_{m,n,t}(q_1, q_2) = (\tfrac{1}{2})^{1/2}[\phi_m(q_1)\phi_n(q_2) + (-1)^t\phi_n(q_1)\phi_m(q_2)],\ m \geq n + t \quad (4)$$

where m, n refer to the order of the Morse oscillator-like functions used in the radial basis set (*11*) and $t = 0$ for the symmetric combination and $t = 1$ for the asymmetric combination. Both m and n were allowed to take values up to 23. The angular coordinate $\theta = (\mathbf{A}_1\hat{\mathbf{Q}}\mathbf{A}_2)$ was represented by Legendre polynomial functions up to order 80.

For all three molecules, all the band origins reported here were converged to 1 cm^{-1} or better. The fundamentals were converged to 0.01 cm^{-1}. Optimized parameters for the radial basis functions are given in Table I.

The rotationally excited $J > 0$ calculations were performed by first computing the lowest 400 non-Coriolis coupled functions for each value of k from 0 to J as an

TABLE I

Optimized Parameters Used in Radial Basis Functions

Molecule	Co-ordinate	R_e/a.u.	ω_e/a.u.	D_e/a.u.
H_2S	q_{HS}	2.750	0.010	0.100
D_2S	q_{DS}	2.600	0.009	0.100
HDS	q_{HS}	2.580	0.008	0.100
	q_{DS}	2.610	0.012	0.100

intermediate basis set. The final basis was then composed of $(J + 1) \times 150$ functions chosen from the intermediate basis on energy ordering (*8*). (N.B.: Eigenfunctions of odd Wang, time-reversal, parity require basis functions with k from -1 to $-J$ which, in our basis, are identical to within a phase factor to the functions with k positive.)

This gave rotationally excited levels for which the fully coupled rotation–vibration part of the calculation was converged to 0.001 cm^{-1} for the fundamental manifolds for $J = 1$–15, for all values of K_a and K_c. The energy levels reported here are an accurate representation of the Senekowitsch *et al.* surface.

As well as studying the deuterated isotopomers of H_2S, this work is also, therefore, a useful test of the efficiency of Radau coordinates for calculating fairly highly excited rotational levels. For future studies of dihydride systems and their deuterated isotopomers, in which even more highly excited rotational levels will be required (as in astrophysical applications), we consider that the use of Radau coordinates will prove extremely useful for the production of accurate, converged eigenenergies and wavefunctions.[1]

The Sutcliffe–Tennyson Hamiltonian (*10*) currently employed has to embed the molecular-fixed z axis along one or the other of the radial coordinates. When using either Radau or bond-length, bond-angle coordinates, therefore, it is not possible to keep the C_{2v} symmetry of an AB_2 molecule such as D_2S for calculations with $J > 0$. Instead, wavefunctions corresponding to *ortho* and *para* spin states are computed together.

2.2. *Transition Moments and Linestrengths*

The rovibrational wavefunctions generated in the above calculations were used to compute dipole transition moments and linestrengths (*9, 12*) for D_2S and HDS. Care was taken to ensure that nuclear spin statistics were properly included in the calculations of intensities.

[1] During the course of the calculations on HDS, an error in the TRIATOM modules TRIATOM and SELECT, as published in Ref. (*9*), was detected. β of Eq. (3) had been programmed as $1 - \beta$. This error has been corrected, and updated copies of these programs may be obtained from the authors on request. Please note, this error does not affect calculations on AB_2 molecules.

3. BAND ORIGINS

3.1. Spectroscopic Constants

The spectroscopic constants calculated by perturbation theory are presented in Tables II and III for D_2S and HDS. D_2S is an oblate asymmetric rotor with a value of $\kappa = 0.350$ compared with 0.504 for H_2S. HDS is a prolate asymmetric rotor with $\kappa = -0.489$. In Table IV, we compare the fundamental band origins and leading rotational constants in both species with those measured by Camy-Peyret *et al.* (*5–7*). Agreement with experiment is similar to that obtained for H_2S.

In Table IV we have arranged the band origins and integrated intensities for the

TABLE II

Vibrational Constants of D_2S and HDS (Perturbation Theory Calculations)

	D_2S	HDS
ω_1 / cm^{-1}	1956.9	1962.7
ω_2 / cm^{-1}	885.3	1073.3
ω_3 / cm^{-1}	1968.3	2734.0
x_{11} / cm^{-1}	-14.5	-28.6
x_{22} / cm^{-1}	- 3.2	- 4.8
x_{33} / cm^{-1}	-14.6	-55.5
x_{12} / cm^{-1}	-10.4	-11.7
x_{13} / cm^{-1}	-57.0	- 1.3
x_{23} / cm^{-1}	-12.0	-21.8
$G(000)$ / cm^{-1}	2337.3	2854.1
γ^a / cm^{-1}	-28.3	0.4
ζ_{12}^b	0.00000	0.57763
ζ_{13}^b	0.03519	-0.01286
ζ_{23}^b	-0.99938	0.81619
α_1^A / cm^{-1}	0.058	0.011
α_2^A / cm^{-1}	-0.145	-0.268
α_3^A / cm^{-1}	0.089	0.305
α_1^B / cm^{-1}	0.052	0.105
α_2^B / cm^{-1}	-0.055	-0.081
α_3^B / cm^{-1}	0.030	0.001
α_1^C / cm^{-1}	0.030	0.042
α_2^A / cm^{-1}	0.024	0.035
α_3^A / cm^{-1}	0.018	0.031

[a] Note that $\gamma = \frac{1}{2}k_{1133}$, where k_{1133} is the Darling–Denison constant defined by Mills and Robiette in Ref. (*15*).

[b] Coriolis constant.

TABLE III

Rotational Constants for D_2S and HDS (Perturbation Theory Calculations)

	D_2S	HDS
R_e^{SD} / Å	1.3355	1.3355
R_e^{SH} / Å		1.3355
$\alpha_e^{DSD/H}$ / degrees	92.227	92.227
A_e / cm^{-1}	5.4982	9.7700
B_e / cm^{-1}	4.5178	4.9388
C_e / cm^{-1}	2.4800	3.2805
κ	0.350	-0.489
$10^2\times \tau_{AAAA}$ / cm^{-1}	-0.20806	-0.23901
$10^2\times \tau_{BBBB}$ / cm^{-1}	-0.11129	-0.05268
$10^2\times \tau_{CCCC}$ / cm^{-1}	-0.00640	-0.01230
$10^2\times \tau_{AABB}$ / cm^{-1}	0.10044	0.01002
$10^2\times \tau_{BBCC}$ / cm^{-1}	-0.01310	-0.02211
$10^2\times \tau_{CCAA}$ / cm^{-1}	-0.01207	-0.02252
$10^3\times D_J$ / cm^{-1}	0.26246	0.04117
$10^3\times D_JK$ / cm^{-1}	-0.43819	1.13122
$10^3\times D_K$ / cm^{-1}	0.19174	-0.57488
$10^3\times R6$ / cm^{-1}	-0.06836	-0.02002
$10^3\times \delta_J$ / cm^{-1}	-0.06049	0.02524
$10^3\times \Delta_J$ / cm^{-1}	0.39919	0.08122
$10^3\times \Delta_JK$ / cm^{-1}	-1.25855	0.89095
$10^3\times \Delta_K$ / cm^{-1}	0.87537	-0.37465
$10^3\times \delta_K$ / cm^{-1}	1.41881	0.54663

lowest 60 vibrational modes for H_2S, D_2S, and HDS according to band type. Assignments were made on the basis of wavenumbers and transition moments between the bands in question. In this section we will comment only on the wavenumbers of the band origins.

Expected mass effects reduce the wavenumbers of the bending only modes from H_2S to HDS to D_2S. We have grouped modes involving the stretches according to the total number of ν_1 plus ν_3 quanta, n_s. For $n_s = 1$, we have bands with ν_2, the number of ν_2 bending quanta, ranging from 0 to 7.

3.2. Local versus Normal Mode Description

Dihydride systems have been the focus of considerable attention (*14, 15*) with the respect to the appropriate description of the overtone stretching modes. Child and Halonen, in particular, have drawn attention to the fact that H_2S and H_2Se are very close to the local mode limit (*14*).

TABLE IV

Comparison of Computed and Experimental[a] Constants of D_2S and HDS (Perturbation Theory Calculations)

	D_2S		HDS	
	Computed	Experimental	Computed	Experimental
(0,0,0)				
z.p.e. / cm^{-1}	2377.3		2854.1	
A_0 / cm^{-1}	5.4961	5.4917	9.7699	9.7518
B_0 / cm^{-1}	4.5210	4.5126	4.9390	4.9321
C_0 / cm^{-1}	2.4790	2.4418	3.2803	3.2257
(1,0,0)				
ν_1 / cm^{-1}	1894.1	1896.4	1904.6	
A_1 / cm^{-1}	5.4110	5.4363	9.7533	
B_1 / cm^{-1}	4.4391	4.4647	4.7804	
C_1 / cm^{-1}	2.4345	2.4165	3.2181	
(0,1,0)				
ν_2 / cm^{-1}	867.6	855.4	1038.8	1032.7
A_2 / cm^{-1}	5.7154	5.6250	10.1722	10.0271
B_2 / cm^{-1}	4.5996	4.5866	5.0602	5.0246
C_2 / cm^{-1}	2.4445	2.4214	3.2274	3.1913
(0,0,1)				
ν_3 / cm^{-1}	1904.7	1910.2	2611.4	
A_3 / cm^{-1}	5.3645	5.4055	9.3119	
B_3 / cm^{-1}	4.4728	4.4867	4.9380	
C_3 / cm^{-1}	2.4527	2.4266	3.2342	

[a] D_2S and HDS ground state constants from Ref. 5.
D_2S ν_1, ν_2 and ν_3 constants from Ref. 6.
HDS ν_2 constants from Ref. 7.

In Table V we have given band assignments in both local and normal mode notation, and it is useful to analyze the computed eigenenergies and wavefunctions to ascertain which description is more appropriate for our calculations. For these AB_2 systems we are suggesting that the labeling convention for local modes should place the local mode quantum numbers and symmetry (+ for A_1 and − for B_2, in the C_{2v} point group) in square brackets and the bend quantum number in parentheses, thus $[n_1, n_2, \pm](v_2)$. In addition, we have also changed the normal mode ordering of the levels of H_2S from that given in Ref. (*1*), which was in error in several places, so that it now accords with the more usual ordering.

The Morse oscillator-like basis functions used in the TRIATOM suite to represent the radial coordinate dynamics are essentially local mode functions. Normal modes should then be produced, in so far as they are relevant, as the appropriate combinations of these basis functions.

TABLE V

Vibrational Term Values, G, and Vibrational Band Intensities from the Ground State for H_2S and Isotopomers (The Intensities Were Calculated at 300 K, with Powers of 10 in Brackets; Variational Calculations)

Local mode	Normal mode	H_2S		D_2S		HDS	
$[n_1,n_2](v_2)$	(ν_1,ν_2,ν_3)	G (cm^{-1})	S_b ($atm^{-1}\ cm^{-2}$)	G (cm^{-1})	S_b ($atm^{-1}\ cm^{-2}$)	G (cm^{-1})	S_b ($atm^{-1}\ cm^{-2}$)
[0,0] (1)	(0,1,0)	1190.4	2.65(+0)	860.4	1.60(+0)	1039.2	2.17(+0)
[0,0] (2)	(0,2,0)	2372.0	3.23(-1)	1716.6	1.14(+1)	2071.9	1.77(-1)
[0,0] (3)	(0,3,0)	3543.5	4.18(-2)	2568.0	1.09(-2)	3097.3	5.73(-2)
[0,0] (4)	(0,4,0)	4703.7	2.46(-3)	3414.1	3.55(-4)	4114.6	9.71(-4)
[0,0] (5)	(0,5,0)	5851.6	1.28(-4)	4254.7	1.85(-5)	5123.0	8.09(-6)
[0,0] (6)	(0,6,0)	6986.3	2.67(-6)	5089.2	3.61(-7)	6122.0	3.10(-7)
[0,0] (7)	(0,7,0)	8106.9	3.60(-8)	5917.4	8.84(-9)	7110.7	5.40(-9)
[0,0] (8)	(0,8,0)	9212.5	7.32(-10)	6738.8	2.30(-10)	8088.7	3.71(-10)
[0,0] (9)	(0,9,0)	10302.1	9.84(-12)	7553.2	7.47(-12)	9055.9	3.81(-11)
[1,0+] (0)	(1,0,0)	2620.4	1.40(+0)	1900.6	6.68(-1)	1905.9	6.70(-1)
[1,0-] (0)	(0,0,1)	2631.0	1.54(+0)	1912.0	6.73(-1)	2625.6	1.56(+0)
[2,0+] (0)	(2,0,0)	5154.2	3.60(-1)	3760.4	1.18(-1)	3762.2	2.00(-1)
[2,0-] (0)	(1,0,1)	5155.5	6.12(-1)	3763.2	2.69(-1)	4530.2	3.45(-2)
[1,1] (0)	(0,0,2)	5251.2	3.65(-2)	3814.4	3.86(-3)	5155.3	4.73(-1)
[3,0+] (0)	(3,0,0)	7589.3	1.01(-2)	5569.2	1.91(-3)	7058.8	2.08(-3)
[3,0-] (0)	(2,0,1)	7589.4	3.01(-2)	5569.6	9.98(-3)	6384.9	1.65(-3)
[2,1+] (0)	(1,0,2)	7768.4	5.76(-3)	5658.1	1.01(-3)	5569.2	5.89(-3)
[2,1-] (0)	(0,0,3)	7789.3	5.55(-3)	5679.7	1.41(-3)	7591.6	2.44(-2)
[4,0+] (0)	(4,0,0)	9929.0	8.10(-4)	7331.4[a]	1.32(-4)	8912.5	7.95(-7)
[4,0-] (0)	(3,0,1)	9929.0	4.21(-4)	7331.4[a]	1.38(-4)	8189.7	8.11(-5)
[3,1+] (0)	(2,0,2)	10208.3	2.82(-4)	7468.5	4.17(-5)	7326.7	1.85(-4)
[3,1-] (0)	(1,0,3)	10212.0	5.00(-5)	7476.1	8.12(-5)	9562.7	7.95(-5)
[2,2] (0)	(0,0,4)	10308.8	1.69(-5)	7529.6	1.02(-5)	10010.9	9.15(-7)
[1,0+] (1)	(1,1,0)	3794.6	1.77(+0)	2752.5	6.88(-1)	2934.8	1.33(+0)
[1,0-] (1)	(0,1,1)	3799.8	4.04(+0)	2761.3	1.55(+0)	3645.6	2.44(+0)
[1,0-] (2)	(0,2,1)	4959.9	5.48(-2)	3606.4	1.56(-4)	4659.5	2.12(-2)
[1,0+] (2)	(1,2,0)	4960.1	6.39(-3)	3600.2	7.67(-4)	3957.2	1.61(-2)
[1,0-] (3)	(0,3,1)	6110.2	2.30(-3)	4446.8	4.19(-4)	5666.2	1.41(-3)
[1,0+] (3)	(1,3,0)	6115.6	2.07(-3)	4443.3	3.50(-4)	4972.4	1.13(-3)
[1,0-] (4)	(0,4,1)	7249.4	3.92(-5)	5282.0	3.58(-6)	6665.0	3.76(-5)
[1,0+] (4)	(1,4,0)	7259.8	5.26(-5)	5281.2	4.88(-6)	5979.5	2.66(-5)
[1,0-] (5)	(0,5,1)	8376.5	2.69(-7)	6111.7	9.79(-11)	7655.2	4.27(-7)
[1,0+] (5)	(1,5,0)	8391.6	1.13(-5)	6113.4	1.01(-6)	6977.7	2.64(-7)
[1,0-] (6)	(0,6,1)	9490.6	4.65(-10)	6935.5	2.46(-10)	8636.1	7.14(-10)
[1,0+] (6)	(1,6,0)	9510.2	2.64(-8)	6939.6	1.98(-8)	7966.4	8.23(-9)
[1,0-] (7)	(0,7,1)	10590.9	3.65(-11)	7752.9	5.35(-11)	9607.1	2.00(-9)
[1,0+] (7)	(1,7,0)	10614.6	1.00(-8)	7759.4	8.60(-10)	8944.9	3.76(-10)
[2,0+] (1)	(2,1,0)	6307.7	4.65(-2)	4602.1	1.38(-2)	4780.9	5.97(-2)
[2,0-] (1)	(1,1,1)	6307.7	3.09(-1)	4603.9	8.32(-2)	5539.6	1.14(-3)
[1,1] (1)	(0,1,2)	6403.0	3.06(-5)	4654.2	1.95(-5)	6156.2	1.33(-1)
[2,0-] (2)	(1,2,1)	7451.5	4.72(-3)	5440.5	8.29(-4)	6542.8	5.22(-4)

[a] These band origins are only accurate to $1 cm^{-1}$.

TABLE V—*Continued*

Local mode	Normal mode	H_2S		D_2S		HDS	
$[n_1, n_2](v_2)$	(ν_1, ν_2, ν_3)	G (cm^{-1})	S_b ($atm^{-1}\ cm^{-2}$)	G (cm^{-1})	S_b ($atm^{-1}\ cm^{-2}$)	G (cm^{-1})	S_b ($atm^{-1}\ cm^{-2}$)
[2,0+] (2)	(2,2,0)	7452.1	1.26(-4)	5439.6	5.06(-5)	5793.2	3.08(-4)
[1,1] (2)	(0,2,2)	7546.9	4.71(-5)	5490.1	4.26(-6)	7151.1	1.25(-3)
[2,0-] (3)	(1,3,1)	8585.3	2.71(-4)	6272.4	1.90(-5)	7539.0	2.18(-5)
[2,0+] (3)	(2,3,0)	8585.9	6.86(-5)	6272.2	5.77(-6)	6798.3	4.24(-5)
[1,1] (3)	(0,3,2)	8681.5	1.20(-5)	6321.7	1.25(-6)	8139.2	4.36(-5)
[2,0-] (4)	(1,4,1)	9707.9	1.03(-5)	7099.1	5.21(-7)	8527.4	5.35(-7)
[2,0+] (4)	(2,4,0)	9708.0	1.05(-7)	7099.3	6.64(-8)	7795.4	1.15(-6)
[1,1] (4)	(0,4,2)	9805.6	1.09(-6)	7148.4	5.48(-8)	9119.9	6.65(-7)
[2,0+] (5)	(2,5,0)	10817.4	2.80(-7)	7920.6	5.83(-8)	8783.7	5.75(-9)
[2,0-] (5)	(1,5,1)	10818.2	5.28(-7)	7920.3	1.21(-10)	9507.0	6.14(-9)
[1,1] (5)	(0,5,2)	10917.9	3.39(-7)	7969.9	1.30(-8)	10093.2	6.28(-7)
[3,0-] (1)	(2,1,1)	8723.0	1.34(-2)	6400.7	1.49(-3)	7384.0	3.36(-5)
[3,0+] (1)	(3,1,0)	8723.1	1.85(-3)	6400.6	6.65(-4)	8049.0	2.47(-5)
[2,1+] (1)	(1,1,2)	8906.9	1.44(-5)	6491.0	6.29(-6)	6578.0	1.45(-2)
[2,1-] (1)	(0,1,3)	8917.4	1.47(-5)	6507.8	1.09(-7)	8578.1	6.13(-3)
[3,0-] (2)	(2,2,1)	9847.8	3.77(-4)	7228.8	2.50(-5)	8376.9	1.28(-6)
[3,0+] (2)	(3,2,0)	9848.0	1.53(-5)	7227.8	5.85(-6)	9033.2	3.65(-6)
[2,1+] (2)	(1,2,2)	10037.4	6.46(-7)	7320.2	4.66(-7)	7580.3	1.81(-5)
[2,1-] (2)	(0,2,3)	10037.4	9.76(-7)	7331.4	1.12(-7)	9562.1	3.14(-7)

In Fig. 2 we have plotted the wavefunctions for HDS for the $n_s = 4$ vibrational levels as a function of the radial coordinates (where n_s is the total number of stretch—symmetric plus asymmetric—quanta in the mode), with the angle θ frozen at its ground state equilibrium value.

A node in the wavefunction occurs where the amplitude changes sign and corresponds to one quantum of excitation. Nodes at right angles to one or the other of the radial coordinates represent excitations localized in that coordinate. These represent local modes. Nodes at right angles to the line bisecting the angle between the two axes (i.e., at 45° clockwise to q_1) represent even linear combinations of the two local modes, and nodes parallel to this line, odd combinations.

The plots shown in Fig. 2 all have nodes perpendicular to the radial axes, indicating that the mode involves only excitation of one or the other of the two radial coordinates, i.e., that it is local. This is as expected from the large frequency difference between ν_1 and ν_3 that results from the difference in mass between hydrogen and deuterium.

Analysis of the vibrational wavefunctions for H_2S and D_2S are more difficult. In both these cases, it was appropriate to use the radial basis symmetrization described in Section 2. Wavefunctions for the $n_s = 4$ manifold of D_2S are shown in Fig. 3.

The use of nodal structure to determine local mode versus normal mode character is not straightforward, since for both descriptions nodes may occur at right angles or parallel to the line bisecting the angle between the radial coordinates. In both descriptions, nodes at right angles to the 45° line represent symmetric combinations—in

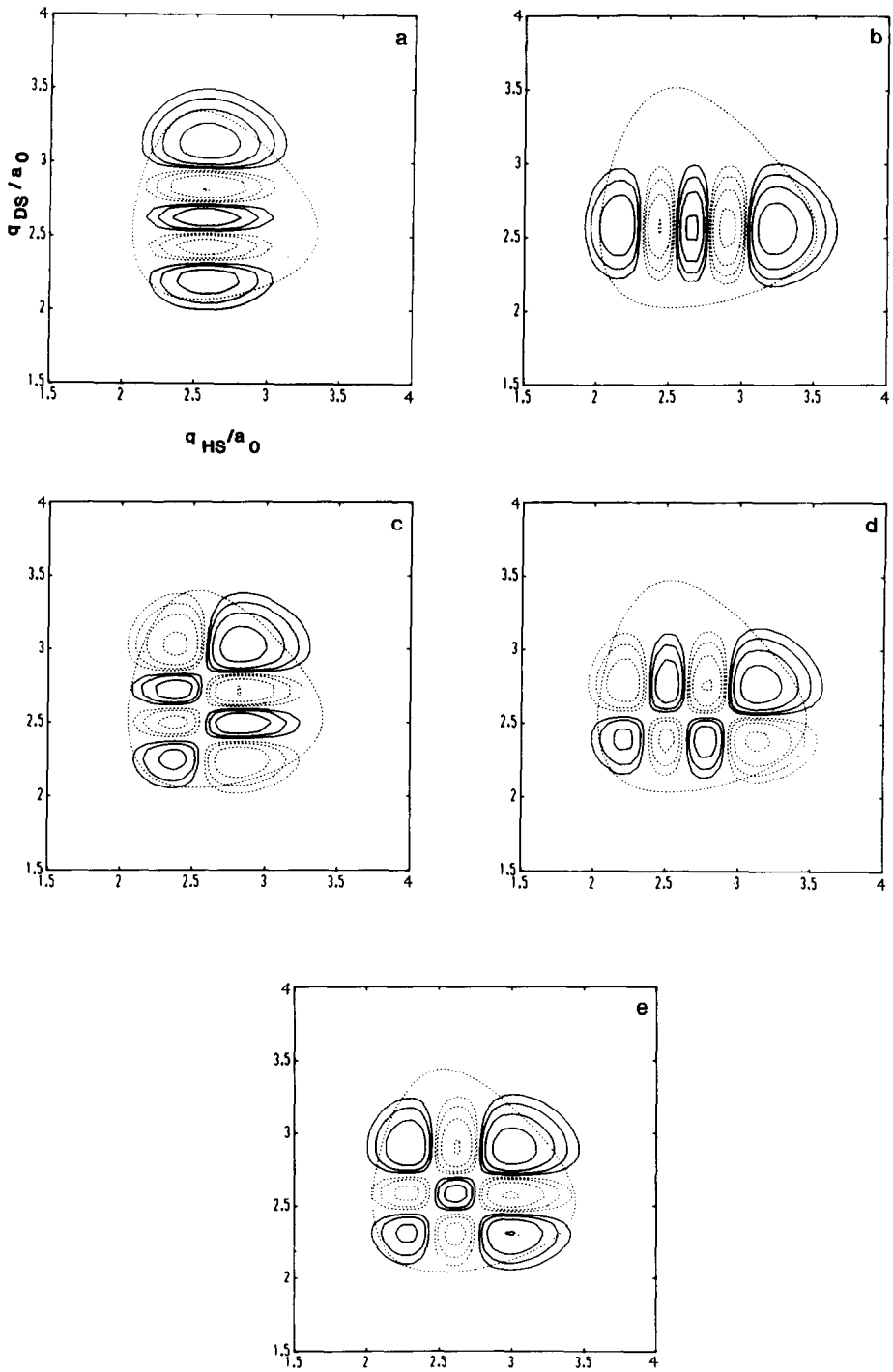

FIG. 2. Plots of the wavefunctions for the $n_s = 4$ manifold for HDS. Contours are given for 64, 32, 16, and 8% of the maximum amplitude of the wavefunction. The solid line countours enclose regions where the wavefunction has positive amplitude, and the broken lines, negative. The outer contour is the classical turning point for the relevant eigenenergy. Plots are in Radau coordinates with θ frozen at its equilibrium value of 92°.

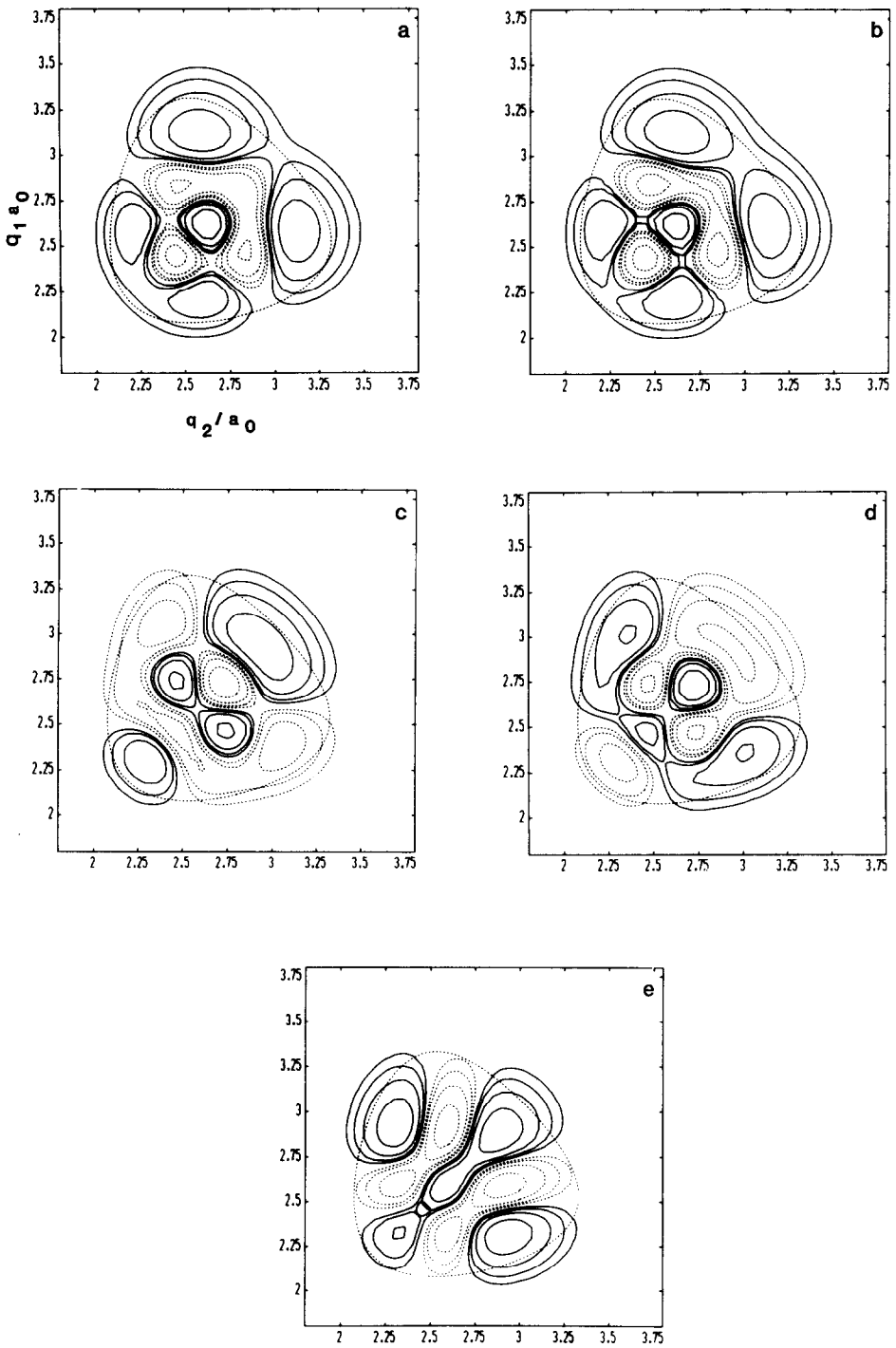

FIG. 3. Plots of the wavefunctions for the $n_s = 4$ manifold for D_2S. See the legend to Fig. 2 for details.

local mode notation the $[n_1, n_2, +]$ combinations, in normal mode notation bands with v_3 even. Nodes parallel to the 45° line are the corresponding asymmetric combinations, $[n_1, n_2, -]$ or bands with v_3 odd. Thus the plots obtained do not distinguish between local and normal mode descriptions, but they do give information about the energy ordering of the final wavefunctions.

To make sense of the resulting states, it is necessary to look at the energy structure of the various n_s manifolds, and the coefficients of the radial basis functions comprising the individual eigenfunctions. Analysis of the energy levels alone indicates that both H_2S and D_2S exhibit almost ideal local mode behavior (*15*). For as low as $n_s = 2$ the two lowest energy levels are almost degenerate and separated by a considerable energy difference from the highest level.

In Table VI we report the result of decomposing the wavefunctions of the $n_s = 2$ and 4 manifolds into their appropriate radial basis components, assuming that the Morse-like functions are identical to local modes. We also include the expected coefficients for the levels in the pure normal mode description.

It is clear from the fact the expected radial basis functions do not account for the whole eigenfunction that the previous assumption is only partly valid. There are two reasons for this. First, the Radau coordinate does not lie along the S–H/D bond, and basis functions in this coordinate are clearly not identical with what is usually considered to be a local mode. The second reason is that states assigned as pure stretch modes do, in fact, contain a considerable amount of bend character.

With these reservations, therefore, the eigenvector analysis broadly confirms the local mode character of the modes concerned. It certainly rules out a pure normal mode description of the states. The plots of the $n_s = 4$ manifold wavefunctions are certainly consistent with this interpretation. In particular, the highest energy level in this manifold shows a nodal structure which is exactly what would be expected from the local [2, 2] designation.

It is notable that the relation predicted by Mills and Robiette (*15*) for the local mode limit, namely $x_{11} = x_{33} = \frac{1}{4}x_{13} = \frac{1}{2}\gamma$ (where γ is the Darling–Dennison parameter, $\gamma = \frac{1}{2}k_{1133}$ in the notation of Mills and Robiette), is obeyed well by both H_2S and D_2S. The corresponding value of the Morse anharmonicity constant x for the SH diatomic moiety is $2x_{11}$ (or $2x_{33}$), i.e., about -29.0 cm^{-1} for D_2S (see Table II).

3.3. Dependence of ν_3/ν_1 Splitting on v_2

Looking only at the homonuclear species, H_2S and D_2S, the levels with 1 quantum of ν_1, v_2 quanta of ν_2, and 0 quanta of ν_3, denoted $(1, v_2, 0)$, are lower in frequency than the $(0, v_2, 1)$ levels only for $v_2 = 0$, 1, and 2. For D_2S, the crossover point comes after $v_2 = 4$.

In fact, a plot of $\Delta^{0,v_2,1}_{1,v_2,0}$ against v_2, where

$$\Delta^{0,v_2,1}_{1,v_2,0} = \nu_{0,v_2,1} - \nu_{1,v_2,0}, \tag{5}$$

is, to a first approximation, a linear function of v_2, given by

$$\Delta^{0,v_2,1}_{1,v_2,0} = A + B \cdot v_2. \tag{6}$$

TABLE VI

Eigenvector Analysis for $n_s = 2$ and 4 for H_2S and D_2S (Variational Calculations)

Local mode basis	H_2S		D_2S		Pure normal mode
	Wavenumber (cm^{-1})	Assignment / Eigenvectors[a]	Wavenumber (cm^{-1})	Assignment / Eigenvectors[a]	
	5154.2	[2,0,+]	3760.4	[2,0,+]	($2\nu_1$)
2,0,+		41 %		89 %	50 %
1,1		7 %		4 %	50 %
	5155.2	[2,0,-]	3763.2	[2,0,-]	($\nu_1 + \nu_3$)
2,0,−		41 %		94 %	100 %
	5251.2	[1,1]	3814.4	[1,1]	($2\nu_3$)
2,0,+		16 %		5 %	50 %
1,1		30 %		89 %	50 %
	9929.1	[4,0,+]	7331.4	[4,0,+]	($4\nu_1$)
4,0,+		68 %		41 %	13 %
3,1,+		0 %		2 %	50 %
2,2		0 %		0 %	37 %
	9929.1	[4,0,-]	7331.4	[4,0,-]	($3\nu_1 + \nu_3$)
4,0,−		69 %		35 %	50 %
3,1,−		0 %		2 %	50 %
	10208.3	[3,1,+]	7468.5	[3,1,+]	($2\nu_1 + 2\nu_3$)
4,0,+		2 %		0 %	75 %
3,1,+		35 %		67 %	0 %
2,2		2 %		0 %	25 %
	10212.0	[3,1,-]	7476.1	[3,1,-]	($\nu_1 + 3\nu_3$)
4,0,−		2 %		0 %	50 %
3,1,−		40 %		75 %	50 %
	10308.3	[2,2]	7529.6	[2,2]	($4\nu_3$)
4,0,+		0 %		0 %	13 %
3,1,+		15 %		8 %	50 %
2,2		39 %		83 %	37 %

[a] Percentages are the proportion of the Morse oscillator-like local mode basis functions occurring in the final eigenfunction. These do not add up to 100% for reasons discussed in text.

For H_2S, $A = 10.4\ cm^{-1}$ and $B = -5.2\ cm^{-1}$. For D_2S, the plot is less well described by a straight line, but we get $A = 11.8\ cm^{-1}$ and $B = -2.4\ cm^{-1}$ (see Fig. 4).

The slope of lines reported here may be explained using the approximate relationship

$$(\nu_n + v_2\nu_2) = \nu_n + (v_2\nu_2) + v_2 \cdot x_{2n}, \tag{7}$$

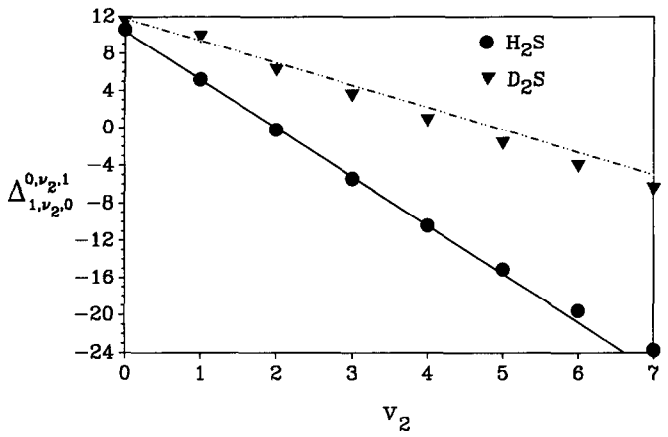

FIG. 4. Plot of the ν_3/ν_1 splitting against ν_2 for H_2S and D_2S. $\Delta^{0,v_2,1}_{1,v_2,0}$ is in cm^{-1}.

where n is 1 or 3, and the terms in parentheses represent the wavenumbers of the combination/overtone bands concerned. Then

$$\Delta^{0,v_2,1}_{1,v_2,0} = \nu_3 - \nu_1 + v_2(x_{23} - x_{21}). \tag{8}$$

For H_2S, $x_{23} = -21.8$ and $x_{21} = -16.4$, giving a slope of -5.4, in good agreement with our findings. But for D_2S, $x_{23} = -12.0$ and $x_{21} = -10.4$, giving a slope of -1.6, rather shallower than the -2.6 our analysis suggests. It is clear, however, that for D_2S, a relatively small increase in x_{23} coupled with a small increase in x_{21} would improve the agreement considerably.

4. INTENSITIES AND SIMULATED SPECTRA

4.1. Band Intensities

Vibrational band intensities (in units of $atm^{-1}\ cm^{-2}$ at $T = 298$ K) are also given in Table V for the band origins presented, calculated from

$$\left(\frac{S_b}{atm^{-1}\ cm^{-2}}\right) = 4.162 \times 10^{-19} \cdot \left(\frac{\omega_b}{cm^{-1}}\right) \cdot \left(\frac{R_b}{D}\right)^2, \tag{9}$$

where ω_b is the band wavenumber and R_b is the vibrational transition moment. The D_2S intensities are, in general, the lowest of the three isotopomers.

In line with the findings of Senekowitsch *et al.*, the bending mode is more intense than either of the two stretches for both D_2S and HDS, with ν_1 more intense than ν_3. Coupling with bending vibration, however, causes the (0, 1, 1) bands to become more intense than the (1, 1, 0) bands for both isotopomers. Where more than one stretching vibration is concerned the tendency is that the mixed ν_1/ν_3 modes are more intense for D_2S and the pure ν_3 modes are stronger for HDS. In this way, the D_2S behavior mirrors that of H_2S.

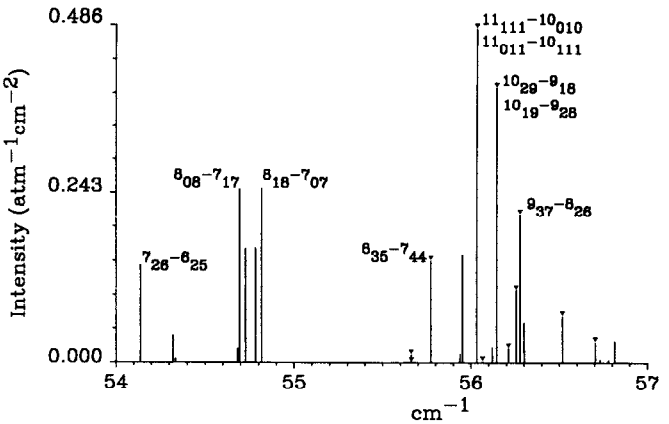

FIG. 5. Computed pure rotational spectrum for an equimolecular mixture of HDS and D_2S at 300 K. Transitions of D_2S are labelled ▼.

4.2. *Rovibrational Transitions*

In Figs. 5 to 8 we present computed spectra for the regions for which Camy-Peyret *et al.* have published detailed spectra (*5–7*). For the pure rotational spectrum of their mixture of HDS and D_2S, our computed spectrum is a good representation in terms of both intensity and line position. In Table VII, we compare our intensities with those reported by Camy-Peyret *et al.* (*5*) for the pure rotational spectra for the most intense lines of Fig. 5.

The wavenumbers are all reproduced to within 0.2 cm^{-1}. Agreement between the computed and experimental intensities is within 7%, probably within the experimental accuracy. At worst, our results indicate that the dipole surface is reproducing the permanent dipole to within 4%. Summing all energy levels up to $J = 15$, we compute the partition functions for D_2S and HDS at 300K to be 1022 and 432, respectively, compared with the experimental values of 1021 and 424 (*5*).

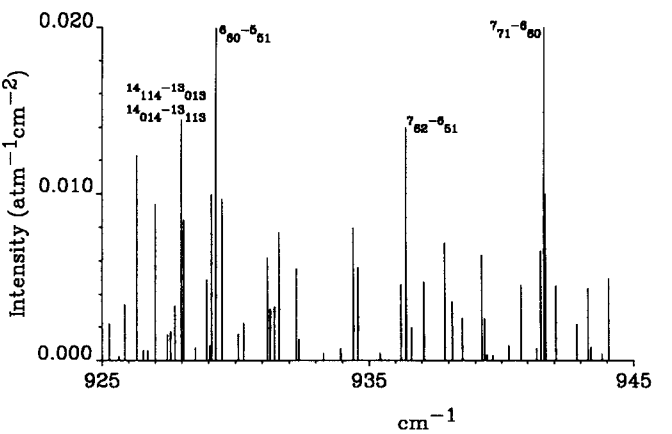

FIG. 6. Computed ν_2 spectrum of D_2S at 300 K.

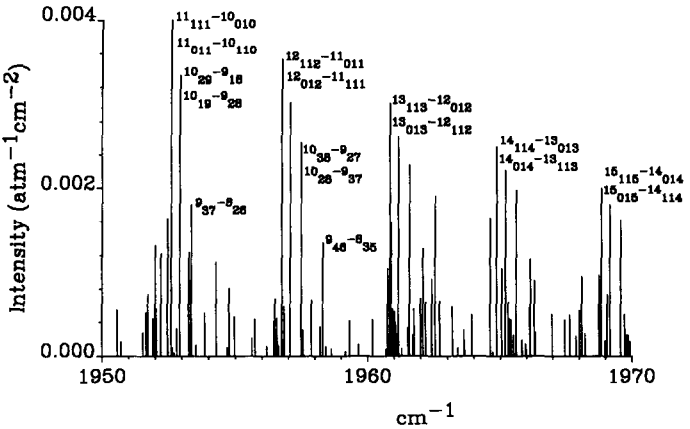

FIG. 7. Computed ν_1/ν_3 spectrum of D_2S at 300 K.

In Figs. 6 to 8 we present sections of the simulated ν_2 and ν_1/ν_3 spectra of D_2S (*6*), and the ν_2 spectrum of HDS (*7*), for comparison with those presented in the experimental reports. The temperature was set to that of the experiment, 300 K. In all cases, the frequency distribution of lines (allowing for correction of the computed band origins) and the relative intensities are well reproduced. Experimental data on the absolute intensities of the rovibrational lines are not available.

Since experimental data on the rovibrational spectra of HDS are still scarce, we present the full ν_2, ν_1, and ν_3 spectra in Figs. 9 to 11. All levels up to and including $J = 15$ have been included. In Table VIII, we have compared line strengths, $S(f - i)$, for a number of transitions for D_2S and HDS. More detailed information is available from the authors on request.

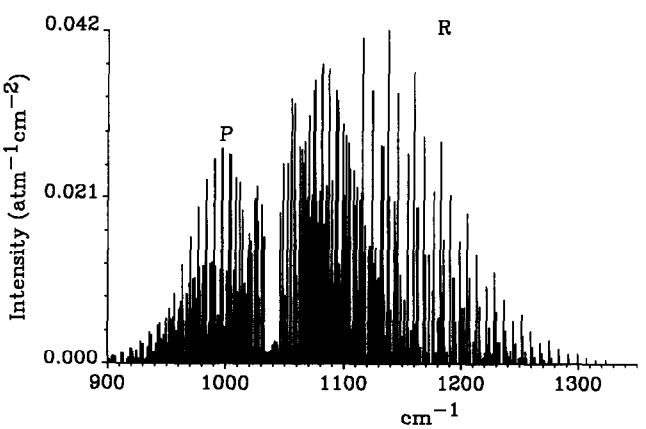

FIG. 8. Detail of the computed ν_2 spectrum of HDS at 300 K.

TABLE VII

Comparison of Computed and Experimental Rotational Transition Wavenumbers and Intensities for D_2S and HDS (Variational Calculations)

	ν_{if} / cm^{-1}		Intensity[a] / $cm.mol^{-1}$	
	Computed	Experimental	Computed	Experimental
HDS				
$7_{26} - 6_{25}$	54.083	54.140	1.05(-20)	9.87(-21)
$8_{08} - 7_{18}$	54.653	54.834	1.99(-20)	1.91(-20)
$8_{18} - 7_{18}$	54.689	54.868	1.23(-20)	1.17(-20)
$8_{08} - 7_{07}$	54.746	54.922	1.23(-20)	1.17(-20)
$8_{18} - 7_{07}$	54.782	54.957	2.00(-20)	1.92(-20)
$7_{16} - 6_{15}$	55.923	56.094	1.16(-20)	1.09(-20)
D_2S				
$8_{35} - 7_{44}$	55.773	55.968	1.23(-20)	1.17(-20)
$11_{011} - 10_{110}$	56.033	56.179	1.32(-20)	1.24(-20)
$11_{111} - 10_{010}$	56.033	56.179	2.65(-20)	2.48(-20)
$10_{19} - 9_{28}$	56.146	56.293	2.19(-20)	2.05(-20)
$10_{29} - 9_{18}$	56.146	56.293	1.09(-20)	1.02(-20)
$9_{37} - 8_{26}$	56.278	56.423	1.77(-20)	1.66(-20)

[a] Powers of ten in brackets.

5. CONCLUSIONS

The potential energy surface developed for H_2S has proved itself to be equally good for the computation of rovibrational energy levels of D_2S and HDS. In the last 3 years Halonen and co-workers (*16, 17*) have developed a potential from spectroscopic data which, coupled with a perturbational Hamiltonian, gives even better agreement with

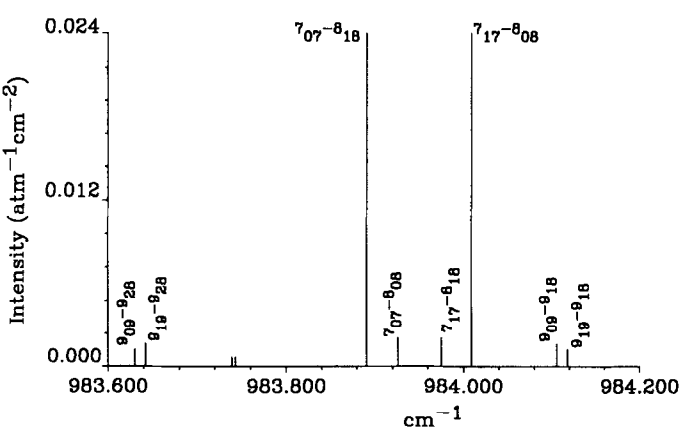

FIG. 9. Full ν_2 spectrum of HDS at 300 K.

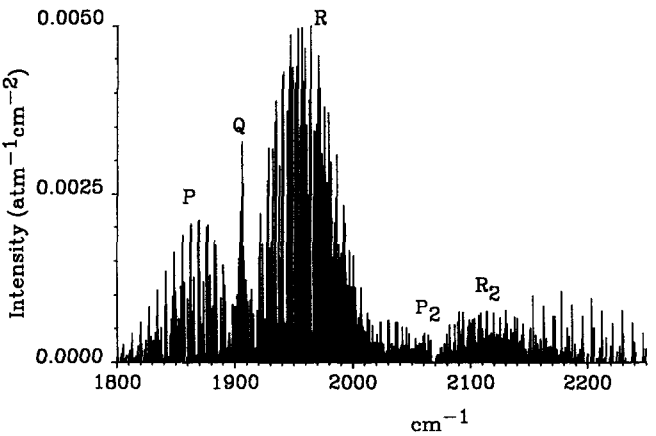

FIG. 10. Full ν_1 (and $2\nu_2$) spectrum of HDS at 300 K.

the measured band origins for the C_{2v} species. Our potential is purely ab initio, however, and has not been adjusted to fit the vibrational data, as was that of Halonen and coworkers.

The drawback of their approach, however, is that the series representing the kinetic energy operator in the Hamiltonian they use is, of necessity, truncated. This, in turn, may have an influence on the terms reported in the potential energy, since these are fitted to the experimental data using the truncated Hamiltonian. One test of the extent to which this might be a problem would be to use the ab initio potential energy surface with the Halonen perturbational approach (or vice versa). From this it might be possible to improve the potential further.

Senekowitsch *et al.* reported that while the dipole surface they calculated was a good representation of the bending coordinate mode, ν_2, it overestimated the strength

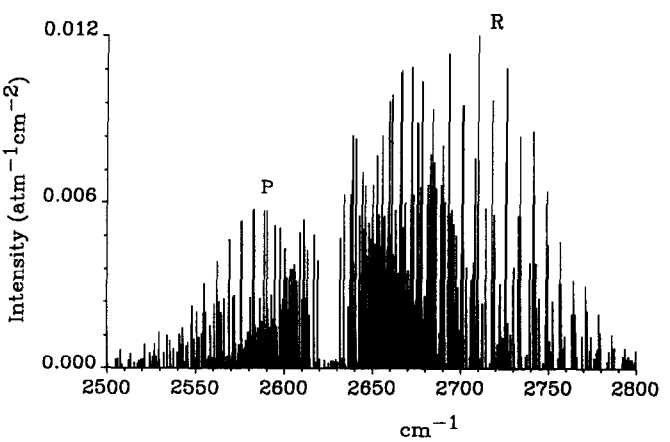

FIG. 11. Full ν_3 spectrum of HDS at 300 K.

TABLE VIII

Sample Rovibrational Transitions for D_2S and HDS (Variational Calculations)

Transition[a]		D_2S		HDS	
J', K_a', K_c'	J'', K_a'', K_c''	ν_{if} / cm^{-1}	$S(f-i)$[b] / D^2	ν_{if} / cm^{-1}	$S(f-i)$[b] / D^2
(010	– 000)				
3 0 3	4 1 4	838.5	5.60(-4)	1008.9	1.47(-3)
2 2 0	2 1 1	865.4	4.17(-4)	1055.5	7.28(-4)
6 2 5	5 1 4	898.3	9.78(-4)	1094.7	1.79(-3)
9 3 6	8 4 5	925.9	1.49(-3)	1098.6	6.58(-4)
(020	– 000)				
3 0 3	4 1 4	1694.7	2.22(-5)	2042.0	1.54(-5)
2 2 0	2 1 1	1722.2	1.41(-5)	2075.1	7.80(-6)
6 2 5	5 1 4	1755.6	2.88(-5)	2129.8	1.90(-5)
9 3 6	8 4 5	1786.6	4.00(-5)	2215.8	4.45(-5)
(100	– 000)				
3 1 3	4 0/1 4	1878.2	7.94(-5)	1877.3	5.91(-5)
2 2 0	2 1/2 1	1904.6	6.05(-5)	1906.5	6.69(-5)
6 2 5	5 1/2 4	1935.8	2.41(-4)	1951.0	1.66(-4)
9 4 6	8 3/4 5	1958.3	3.70(-4)	1975.5	3.18(-4)
(001	– 000)				
3 1 3	4 1/0 4	1889.7	5.66(-5)	2597.6	1.18(-4)
2 2 0	2 2/1 1	1913.0	4.57(-5)	2639.3	7.15(-5)
6 2 5	5 2/1 4	1947.5	6.71(-5)	2677.3	1.98(-4)
9 4 6	8 4/3 5	1969.9	1.34(-4)	2723.1	2.67(-4)

[a] Where two values of K_a are given, the first refers to D_2S.

[b] Powers of ten in brackets.

of the stretch modes (ν_1, ν_3). In the absence of experimental band intensities for either D_2S or HDS, we are not able to test if this is still the case. It would, however, be surprising if it were not so. We conclude that while the intensities we have reported for the pure rotational and ν_2 spectra are probably quite accurate, those involving the stretching modes are almost certainly an overestimation of what would be determined experimentally.

ACKNOWLEDGMENTS

S.M. and J.T. acknowledge financial support from the Science and Engineering Research Council under Grant GR/F/14550. We thank James Henderson for plotting the wavefunctions. P.R. thanks Fonds der Chemischen Industrie and Deutsche Forschungsgemeinschaft for support during the course of this work.

RECEIVED: May 7, 1990

REFERENCES

1. J. SENEKOWITSCH, S. CARTER, A. ZILCH, H-J. WERNER, N. C. HANDY, AND P. ROSMUS, *J. Chem. Phys.* **90**, 783–794 (1989).

2. P. BOTSCHWINA, A. ZILCH, H-J. WERNER, P. ROSMUS, AND E-A. REINSCH, *J. Chem. Phys.* **85,** 5107-5118 (1986).
3. R. L. COOKE, F. C. DE LUCIA, AND P. HELMINGER, *J. Mol. Struct.* **28,** 237–245 (1975).
4. I. M. MILLS, private communication (1989).
5. C. CAMY-PEYRET, J-M. FLAUD, AND L. LECHUGA-FOSSAT, *J. Mol. Spectrosc.* **109,** 300–333 (1985).
6. C. CAMY-PEYRET, J-M. FLAUD, A. N'GOM, AND J. W. C. JOHNS, *Mol. Phys.* **65,** 649–657 (1988).
7. C. CAMY-PEYRET, J-M. FLAUD, A. N'GOM, AND J. W. C. JOHNS, *Mol. Phys.* **67,** 693–695 (1989).
8. J. TENNYSON AND S. MILLER, *Comp. Phys. Commun.* **55,** 149–175 (1989).
9. F. T. SMITH, *Phys. Rev. Lett.* **45,** 1157–1161 (1980).
10. B. T. SUTCLIFFE AND J. TENNYSON, *Int. J. Quantum. Chem.* (in press).
11. J. TENNYSON AND B. T. SUTCLIFFE, *J. Chem. Phys.* **77,** 4061–4072 (1982).
12. S. MILLER, J. TENNYSON, AND B. T. SUTCLIFFE, *Mol. Phys.* **66,** 429–456 (1986).
13. S. CARTER AND N. C. HANDY, *J. Chem. Phys.* **87,** 4294–5007 (1987).
14. M. S. CHILD AND L. HALONEN, *Adv. Chem. Phys.* **57,** 1–58 (1984).
15. I. M. MILLS AND A. G. ROBIETTE, *Mol. Phys.* **56,** 743–765 (1965).
16. L. HALONEN AND T. CARRINGTON, JR., *J. Chem. Phys.* **88,** 4171–4185 (1988).
17. E. KAUPPI AND L. HALONEN, *J. Phys. Chem.* (in press).